Hindawi
Advances in Materials Science and Engineering
Volume 2019, Article ID 6834269, 15 pages
https://doi.org/10.1155/2019/6834269

Research Article

Effects of Stem Cutting in Rice Harvesting by Combine Harvester Front Header Vibration

Zhong Tang, Haotian Zhang, Yuepeng Zhou, and Yu Li

School of Agricultural Equipment Engineering, Jiangsu University, Zhenjiang 212013, Jiangsu, China

Correspondence should be addressed to Zhong Tang; tangzhong2012@126.com

Received 19 October 2018; Accepted 10 January 2019; Published 3 February 2019

Guest Editor: Dariusz Rozumek

In order to reveal the reason of stem cutting in rice harvesting by combine harvester front header, stem cutting principle of the front header was developed. Based on the structural models and the parameters of each part of header, the first eight-order constrained modal simulation analysis was carried out to obtain the vibration response frequency. The front header was produced and used to be tested for restraint experimental modal in the rice field. The rice stem cutting state of the header cutter was analyzed by carrying out the vibration test of the no-load rotation state and rice harvesting state in the field. According to the cutting diagram of the stalk in the header, the angle of the cutting surface and length distribution of the short stalk were analyzed with compound state of forward and vertical vibration. The results showed the mean and variance amplitude of front header were similar to length distribution of the short stalk. The mean length 23.60 mm of the repeatedly cut stems was inextricably linked to the up and down vibration amplitude 25.36 mm of the header. The stem cutting surface angles 38°, 44°, and 62° were for different forward speed and cutting areas on the cutting diagram. The above studies reveal the intrinsic nature between header vibration and length distribution of the cutting stem.

1. Introduction

There are always short rice stalks in the grains after rice is harvested from the field. This problem seriously affects the processing and rice grains' quality in the later stage. The cause of short rice stalks has become a current research topic. The vibration behaviors of many structures are generally identified by the method of analyzing the experimental modalities [1, 2]. The relationship between stem cutting and vibration state has received considerable amount of attention. This is a difficult research to reveal the intrinsic nature between header vibration and short rice stem by investigating the vibration state of rice harvesting machinery.

There is strong vibration at the front header of rice combine harvester, which is induced by the dynamic load and the road surface [3, 4]. Vibration of the cutting platform causes reduction of frame lifetime and driver's comfort and also affects the working precision of the machine. There were many research results on vibration of the combine harvester header [5]. The experimental assessment of the most relevant vibration properties of a combine harvester cutting platform was carried out by Ebrahimi et al. [6]. Chuan-Udom developed 3 types of new cutter bar drivers to reduce the vibration of rice combine harvester [7]. Fukushima et al. revealed that the harmonic frequency components varied with an increase in the width of the interspace although the highest harmonic frequency in the simulation was three times as high as the crank wheel rotation frequency [8, 9]. There are many reasons for front header vibration, such as dynamic loading excitation, natural frequency resonance, and vibration transfer response. Yu et al., took 4LZ-4.6 full-feed harvester's header as research object and adopted the cumulative damage rule to obtain the fatigue life of the header frame [10]. When the excitation frequency was in an integer multiple of the natural frequency of the structure, the vibration of the structure would be excited. Fukushima et al. constructed a dynamic model of the knife driving system to forecast the vibration characteristics of the knife driving system [9]. The vibration occurred at joint of the link arm, and the drive knife was three times as high as the driving frequency.

For the vibration and imbalance problems of the harvester header, the dynamics simulation of the header of the small combine harvester was carried out by Kong et al. [11]. The speed curves of the cutter and the transverse conveyer chain were obtained through dynamic simulation. In order to enhance the process stability of adjusting the height of the header during the operation of combine harvester, a height adaptive adjustment system for the header was developed [12]. Li et al. established a three-dimensional model of the 4LZ-2.0 rice-wheat combine harvester header frame in Solidworks and introduced the model into the ABAQUS finite element analysis software to establish a finite element model [13]. Through the analysis of the modal parameters, the vibration form of the header frame and the weak link of the structure under the excitation frequency were obtained [14]. There were much more studies focused on cutter bar of header. Although many solutions to reduce the vibration of header were also proposed, the vibration in rice cutting process was more obvious and serious. Gao et al. tested the vibration of crawler-type combine harvester in field harvesting condition and indicated that harvesting status caused significant vibration [15]. In order to reduce the vibration of the header in harvesting, Li et al. established a three-dimensional model and performed a finite element modal analysis of the header and bridge of the combine harvester [16]. He carried out reliability optimization design of the wheat harvester header structure [17]. Based on the analysis of the principle of the hydraulic system of the traditional rice harvester, the targeted upgrade was carried out, and the test was verified on test bench. According to the principle of combine harvester, Lu et al. designed a double-cutter double-roller full-track regenerative rice harvester structure [18].

On the contrary, overhigh speed led to too much vibration on the header and caused the reel index to increase header loss. Vibration on the cutter bar driver was measured in some studies at the header's drive axial speed from 250 to 400 rpm. The reel, front auger, and chain conveyer moved along the rice combine harvester's moving direction and caused the relatively low vibration which was compared to that caused by the cutter bar driver [19]. The head structure was optimized by using Pro/E to model and using Matlab to make numerical calculation, and a three-dimensional head model with quality, cross-sectional area, and reliability optimization was established [20]. In order to reduce the harvest loss caused by the vibration of the header during the harvesting process, the motion and dynamic analysis of the cutting transmission system were carried out. The differential equations of the system horizontal vibration were established and solved [21].

Many research results are also obtained. However, for the field working mode of the header, the influence of header vibration on stem cutting and the morphological characteristics left on stalk cut surface was rarely studied. Research results in this area are of great significance for the design of the rice combine harvester header structure.

The objective of this study was to determine vibration behavior of front head of rice combine harvester, structural model, and stem cutting principle of header platform. The designed header structure was manufactured, and a restraint experimental modal test of the header was carried out in rice field. According to the stalk cutting diagram of the header under the horizontal movement of the cutting head and the horizontal movement of the header, the angle of the cutting surface of the stalk generated during the cutting process of the header and the intrinsic essential relationship between the short stalk and the vibration of the header were analyzed.

2. Materials and Methods

2.1. Structure of Front Header. Front header is an important part of rice harvesting to achieve stem cutting and collection [22]. The stalk cut by header is transported from header to threshing cylinder by conveying house. The front header of rice combine harvester consists of header platform, cutting bar, combine auger, pentagon reel, and conveying house. The front header is shown in Figure 1.

As shown in Figure 1, the harvesting process of front header consists of three steps. The first step was to shift stems with pentagon reel, and then the stems were guided into header platform. The second step was to cut stems by cutting bar, and then the stems were separated from root. The third step was to collect and compress the stems, and the stems were fed to threshing cylinder by conveying chain [23]. That is, the function of the front header was the initial preparation work for subsequent grain threshing. In rice harvesting process, there are always short rice stalks in the grains after rice is harvested from the field.

As shown in Figure 1, the pentagon reel radius is 500 mm. The rod number is 5, and the reel eccentric distance is 60 mm. Reel shaft inner and outer diameters of the tube are 36 mm and 42 mm, respectively. Reel wheel speed is 35 r/min. The combine auger diameter is 300 mm, helical blade height is 100 mm, pitch is 460 mm, the speed of feeding auger is 150 r/s, gap between the helical blade and floor is 20 mm, and clearance between helical blade and rear side of cutting table is 25 mm. The spiral cylinder of the cutting table is provided with 11 telescopic fingers. The cutter driving wheel speed is 411 r/min.

2.1.1. Pentagon Reel. The pentagon reel could adjust the movement direction of stem while the combine harvester was going forward. The pentagon reel performed circular motion under rotating condition. So, the trajectory of pentagon reel was a combination of circular motion and linear motion. Structural model of pentagon reel is shown in Figure 2. While the pentagon reel was running, the reel teeth should be always vertically downward. Only in this way, the stem could be pushed into header platform. The method of ensuring the reel teeth being vertically downward was based on the principle of planar four-bar linkage [24].

As shown in Figure 2(b), the O point on pentagon reel was selected as the research object and set as the coordinate origin. The vertical direction was the Y coordinate and the horizontal direction was the X coordinate. The trajectory of O point was a combination of circular motion and linear motion. Then, the trajectory equation of O point is shown as follows:

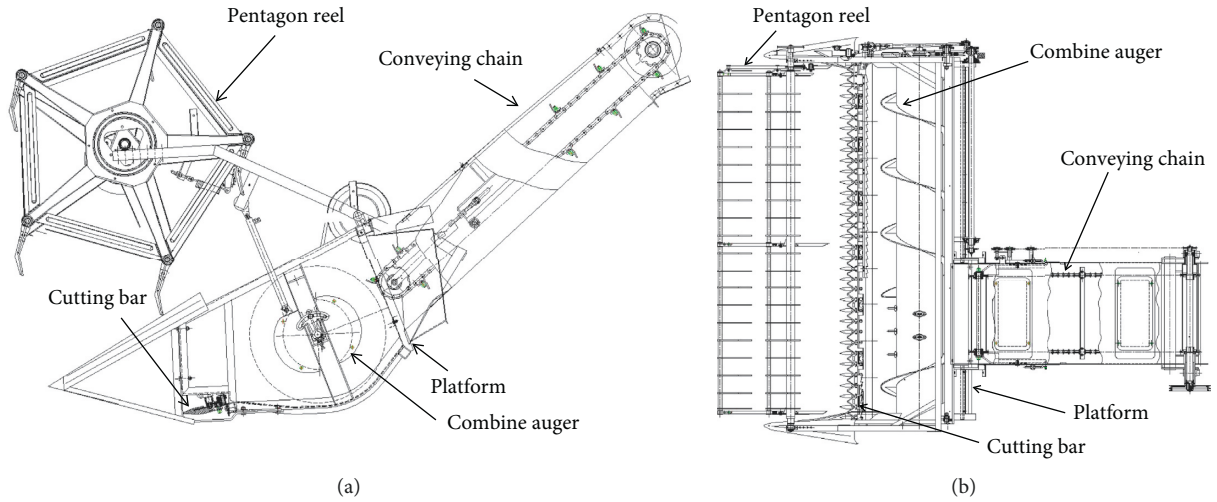

Figure 1: Structure and composition of front header. (a) Header main view. (b) Header top view.

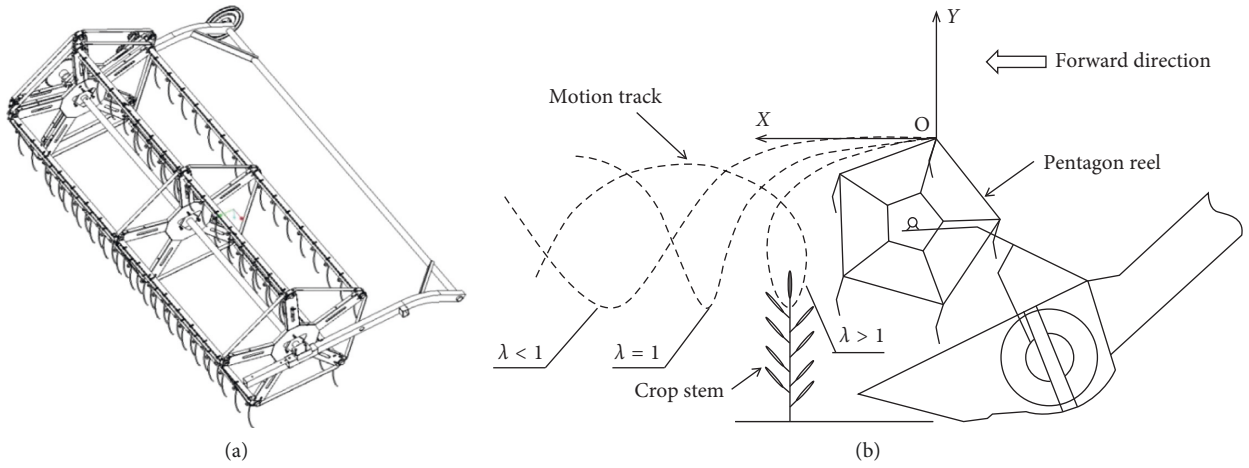

Figure 2: Structure and schematic of the pentagon reel. (a) Assembly of the pentagon reel. (b) Trajectory of the pentagon reel.

$$\begin{cases} X = Vt + R\cos\omega t, \\ Y = H - R\sin\omega t + h, \end{cases} \tag{1}$$

where R is the radius of the reel, ω is the rotational velocity, H is the height from the ground to point O, h is the height from the ground to cutting bars, t is the motion time, and V is the forward velocity of the pentagon reel.

Based on the trajectory equation of O point, the velocity of O point could be obtained by equation (1). The motion velocities of O point in X coordinate and Y coordinate are shown as follows:

$$\begin{cases} V_X = \dfrac{dX}{dt} = -R\omega\sin\omega t + V, \\ V_Y = \dfrac{dY}{dt} = -R\omega\cos\omega t. \end{cases} \tag{2}$$

If the O point of the pentagon reel had to be toggled and guided toward the stem, the horizontal movements' speed of the O point needs to have a value of X negative. Let λ be the ratio of V_y to V (V_y/V). When $\lambda > 1$, $\lambda = 1$, or $\lambda < 1$, the trajectory of O point is shown in Figure 2(b).

As shown in Figure 2(b), when the $\lambda > 1$, the trajectory of O point was a long cycloid. The trajectory formed a buckle, and the bat had a rearward horizontal speed at the lower portion of the buckle. So $\lambda > 1$ could let pentagon reel be toggled and guided toward the stem. In order to reduce the impact of the pentagon reel on the stem, the horizontal velocity of the O point should be zero which was the best state. So, the motion velocity of O point at X coordinate should be as follows:

$$V_X = -R\omega\sin\omega t + V = 0. \tag{3}$$

Then, $\sin\omega t = V/(R\omega) = (\cos\omega t)/\lambda$, $\lambda = (\cos\omega t)/(\sin\omega t) = ctg\omega t$. So, $\lambda = ctg\omega t > 1$ was the factor of horizontal velocity of the O point be zero.

2.1.2. Cutting Bar. The cutting bar was composed of a reciprocating cutter and fixed supporting portion which was riveted by a cutter bar, movable blades, and cutter

heads. During the cutting crop stem process, the cutter reciprocated and the front edge of the edge guard divided the stems into small bundles and led to the cutter. The cutter pushed the straw to the fixed blades for cutting during the movement. The structural model of cutting bar is shown in Figure 3.

The drive mechanism of the cutting bar changed the rotary motion into reciprocating motion. The existing mainstream adopted the principle of the pendulum mechanism. The pendulum ring mechanism converted rotary motion into reciprocating motion by a pendulum ring mounted obliquely on the main shaft and through a swinging shaft. Pendulum drive mechanism of cutting bar is shown in Figure 3(b). The law of blade motion had a direct impact on the performance of the cutter. The cutter stroke of the pendulum ring mechanism can be expressed as follows:

$$L = 2Kl \sin \beta, \tag{4}$$

where L is the cutter stroke of the pendulum ring, K is the correction factor (0~1), l is the pendulum length, and β is the pendulum angle.

Drive components of horizontal cutter used a slew ring transmission mechanism. To facilitate specialized production and spare parts supply, the industry standard specifies a spacing of 76.2 mm between adjacent cutters and a horizontal inclination of 6°30′. The length of pendulum bar was 95 mm, the pendulum ring angle was 22°, the average speed of the cutter generally was 0–1.2 m/s, and the cutter driving wheel speed was 411 r/min [25]. The cutter knife was perpendicular to the heading direction of the harvester (reciprocating motion in horizontal direction).

2.1.3. Combine Auger. The function of combine auger was transferring the cut crop stalks to the feeding inlet of conveying house. There were two parts of spiral blades and telescopic teeth to complete stalk collection and delivery. Spiral blades were mounted on the surface of the cylinder body [26]. Structural model of combine auger is shown in Figure 4(a). Telescopic teeth were eccentric retractable grilled fingers. The feeding inlet function of eccentric retractable grilled fingers is shown in Figure 4(b).

As shown in Figure 4, inner diameter, outer diameter and pitch were major parameters of the combine auger. Circumference length of the inner diameter should be longer than the length of crop stalks to avoid the stalks entangled on the cylinder body. The size of the pitch was determined by the ability of the spiral blade to transport the crop stalk. The pitch S of the auger should be as follows:

$$S \leq \pi\ dt\ g\alpha, \tag{5}$$

where S is the pitch of the combine auger, d is the diameter of the cylinder body, and a is the spiral angle.

As shown in Figure 4, the telescopic fingers were mounted in the spiral barrel and hinged on a fixed crankshaft. The center of the crankshaft had an eccentricity from the center of the spiral cylinder. The outer end of the finger was connected to the spiral barrel through a ball joint. When the spiral barrel rotated through the rotating shaft, it drove the fingers to rotate together. However, due to the disagreement between the two fingers, the fingers referred to the telescopic movement relative to the surface of the spiral cylinder.

2.1.4. Assembly of Front Header. The header platform mainly included structural beams and sealing plates. The header platform was the skeleton and base that bore the loads of pentagon reel, cutting bar, and combine auger. The frame bore the loads of pentagon reel, cutting bar, and combine auger. Structural model of the header platform is shown in Figure 5.

The conveying aisle was a bridge connecting the header frame to the threshing cylinder. The conveying aisle mainly consisted of a carrying frame and a conveyer chain. Structural model of conveying aisle is shown in Figure 6.

According to the industry standard for grain combine harvesters, the length, width, and height of the caries were 560 mm, 21 mm, and 21 mm, respectively. The chain spacing was 35.2~46.3 mm, and the chain speed was 3~5 m/s.

Based on the above design and parameters, the header platform, cutting bar, combine auger, pentagon reel, and conveying chain were assembled. Assembly drawing of front header is shown in Figure 7.

As shown in Figure 7, there are many rotating parts on the header, which was prone to vibrate with low frequency mode [27]. The vibration of the header has a great influence on the cutting of rice stems, which brings great difficulty to the precise control of the stalk height during the stalk cutting process.

2.2. Stem Cutting Principle. The forward speed and cutting frequency of cutting knife were the major factors that affected the efficiency of rice stem cutting. The cutter consisted of moving knife and fixed knife. Fixed knife was welded and relatively stationary with the header frame. The cutting frequency of the moving knife depended on the frequency of the crank. Then, the cutting speed of the moving knife is shown as follows:

$$\mathrm{Vp} = \frac{ns}{30}, \tag{6}$$

where Vp is the cutting speed of the moving knife, n is the cutter crank speed, and s is the stroke of the moving knife.

The forward distance of the front header by the cutter passed a stroke is shown as follows:

$$H = \frac{\pi V}{\omega}, \tag{7}$$

where V is the forward velocity of the front header and ω is the cutter crank angular velocity.

The advancement distance of the header directly affected the area swept by the movable knife on the ground, which is the cutting diagram of the movable knife. The movement of the cutter was synthesized by the forward movement of the head and the reciprocating cutting motion in the horizontal direction. The cutting diagram of the movable knife is shown in Figure 8.

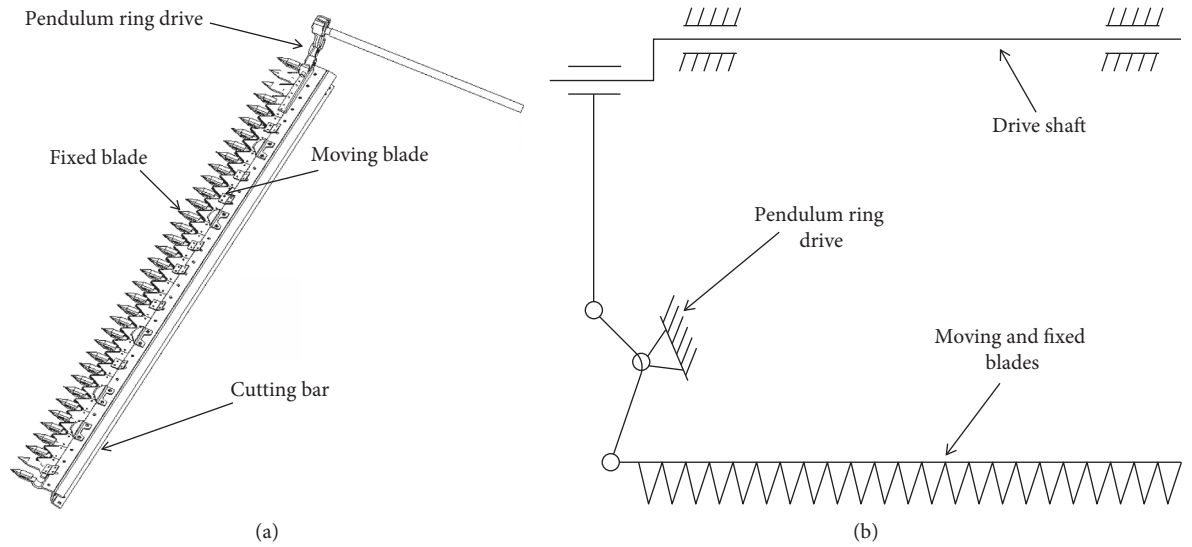

Figure 3: Structure and schematic of the cutting bar. (a) Assembly of the cutting bar. (b) Pendulum drive mechanism.

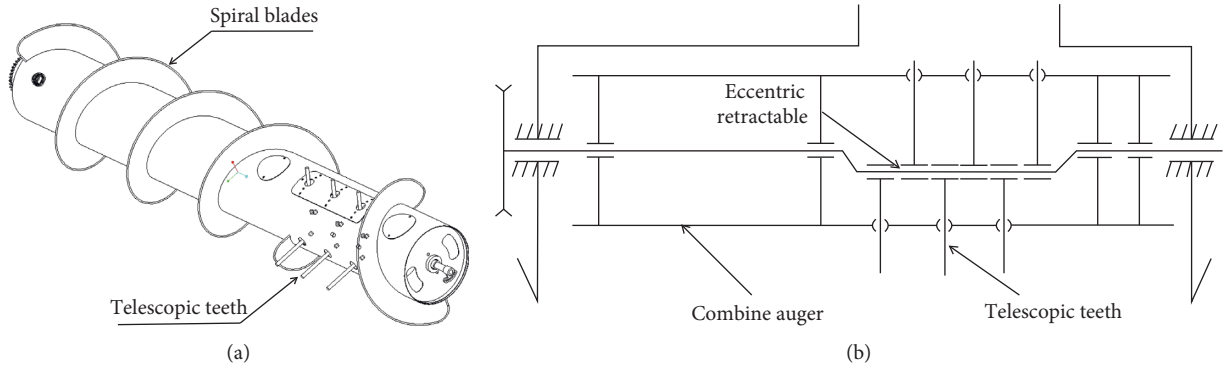

Figure 4: Structure and schematic of the combine auger. (a) Assembly of the combine auger. (b) Eccentric retractable grilled fingers.

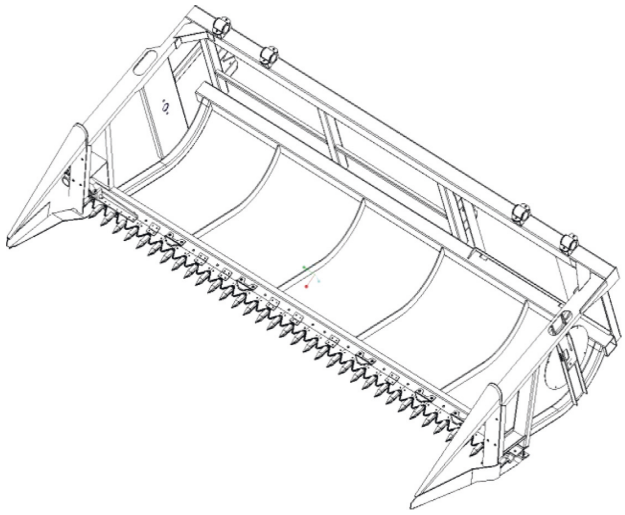

Figure 5: Assembly of the header platform.

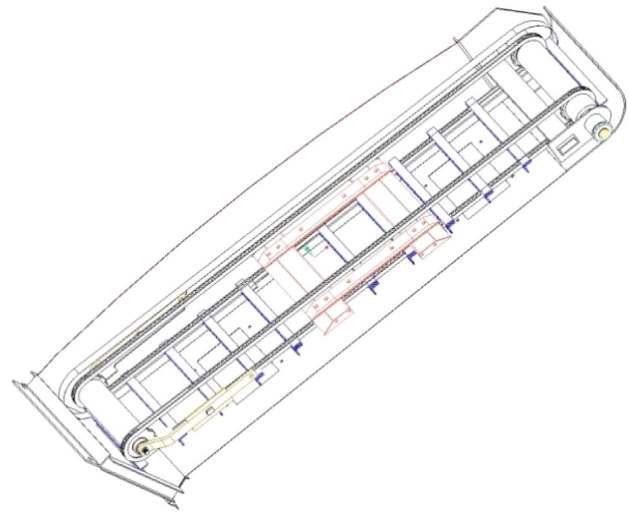

Figure 6: Assembly of conveying chain.

As shown in Figure 8, when moving knife was at position 1, the moving knife and fixed knife were at starting position. When the front header forward and the cutter moved to the right, the movable knife reaches the position 2. The trajectory of moving knife was AB and CD. As the front header forward and the cutter moved to the left, the movable knife reaches the position 3. The trajectory of moving knife was EF and GH. The cutting diagram of movable knife was red shaded area. The red shades from position 1 to position 2 and position 2 to position 3 are visible.

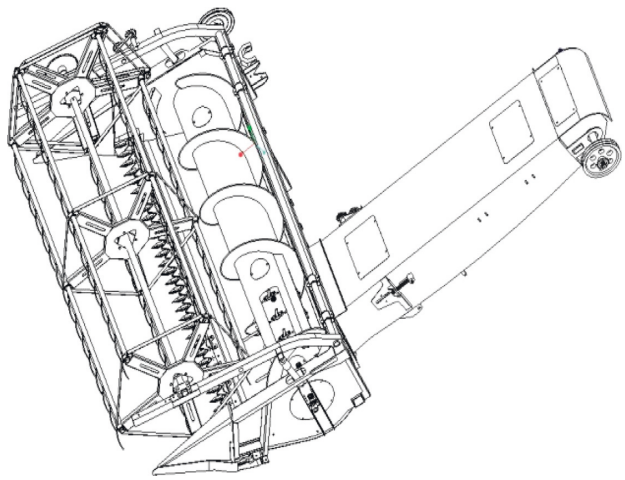

Figure 7: Assembly of the front header.

There were three stem cutting areas, zone I, zone II, and zone III. Zone I was the first cutting area of the moving knife; then, zone I was the first cutting area covered by the moving knife from left to right. As the header moved forward, the moving knife would move from right to left and cover an area, which was named as the second cutting area. Zone II was the first and second cutting overlap area of the moving knife. In zone II, the stem would be cut twice. If the header vibrated up and down, zone II showed presence of repeated cuts, which would result in short stalks. The third zone was the leakage cutting zone during the cutter movement. In the area of the leak-cut zone III, the stem would be pushed forward to the next cutting zone for cutting. The Stem oblique cutting principle is shown in Figure 9.

In zone I, the stem would be cut horizontally and the cutting head of the stem would be horizontal (or 90°). The cut horizontally was shown as OA rice stem. In zone II, the stem would be repeatedly cut to produce short stalks. If the header had vibration up and down, the stem would be cut was as OB rice stem. In zone III, The missing stalk would be pushed to the next cutting area and the stalk would be cut in a slanted state. The stem would be cut was as OC rice stem shown.

2.3. ANSYS Simulation of Front Header. Front header was an assembly device with header platform, cutting bar, combine auger, pentagon reel, and conveying device. The front header's intrinsic mode of dynamic response was an important factor affecting the working state after assembly. The 3D model of the front header was developed by Pro/E and saved as STEP format. Intrinsic modes of front header unit were calculated by ANSYS Workbench [28]. The front header 3D model was gathered and assembled by Pro/E; the assembly model of the front header is shown in Figure 10(a). Then, the 3D model of the front header was imported into ANSYS Workbench and is shown in Figure 10(b).

In order to ensure the free lifting and loading of the front header, the end of the front header was connected to threshing cylinder frame by bearing constraint. The hydraulic cylinder was supported in the middle of the lower side of the conveyer house. The load of the front header was applied to threshing cylinder frame and hydraulic cylinder which were located on the chassis frame. The two fixed constraint positions A and B beams of the front header were threshing the cylinder frame and hydraulic cylinder on the chassis frame, respectively. The two fixed constraint positions are shown in Figure 11(a).

Front header is mainly welded from Q235 structural steel, angle steel, and square steel. Then, the 3D model was imported into ANSYS Workbench. The material properties selected during ANSYS analysis are elastic modulus $E = 210$ GPa, Poisson's ratio $\mu = 0.33$, density $\rho = 7850\ \text{kg/m}^3$, and yield strength $\sigma_s = 235$ MPa. Because the minimum thickness was 2 mm, the grid size was 2 mm in automatic and swept meshing method. The total number of nodes in the finite element simulation model is 155824. The meshing result is shown in Figure 11(b).

2.4. Experiment Mode of Assembly Front Header. According to the model of header platform, cutting bar, combine auger, pentagon reel, and conveying chain, the front header physical map was processed. The front header of rice combine harvester is shown in Figure 12. The header platform and conveyer aisle were bearer frame. All incentives were applied to the frame. The modality of front header frame was an important factor reflecting the bearing and vibration response of the header.

In order to obtain the experimental mode of header platform and conveyer house, the DH5902 dynamic signal acquisition instrument was used to test the experimental mode. The signal acquisition system and dynamic signal acquisition instrument were produced by Chinese Donghua testing company. The test system consists of vibration signal acquisition system and signal analysis processing system, as shown in Figure 13. The signal acquisition system collected the electrical signal of acceleration on frame under different conditions. Signal acquisition system used the United States of America (PCB) 356A16 type three-component acceleration sensors to test the vibration signals. The methods for testing and analyzing experimental modalities were available in Reference [29].

In order to test the modals of header platform and conveyer aisle, the structure of header platform and conveyer aisle was reduced to a 24-points frame model. The line model is shown in Figure 14(a), and the contour model is shown in Figure 14(b).

The single-input and multi-output method was used to test the modes of header platform and conveyer aisle. Four 356A16 type three-component acceleration sensors were arranged in batches to test the vibration response of 24 points of the header platform. The 13 channels received the excitation signal of the test hammer and the vibration signals of the acceleration sensors.

2.5. Frame Vibration Test of Front Header. In order to analyze the vibration characteristics of the front header in the field, the influence of the vibration characteristics of the header platform with the rice stems cutting was obtained. Two points on the header frame were selected to characterize the vibration of the front header when the rice stem was cut. The vibration of the Point 1 (P1) and Point 2 (P2) represented the cutter bar cutting the rice stem when the header vibrated. Two vibration test points of front header are shown in Figure 15.

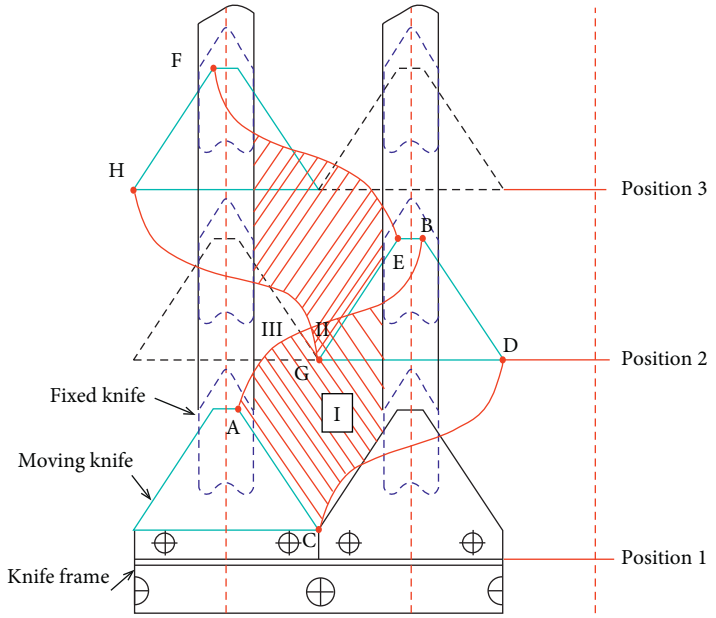

Figure 8: Cutting diagram of the movable knife.

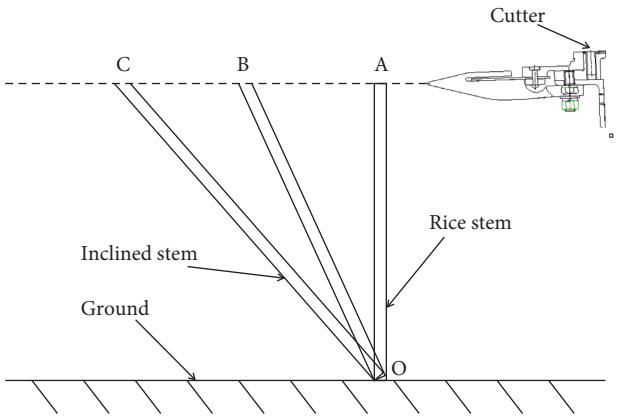

Figure 9: Stem oblique cutting principle.

When the combine harvester was working in the field, the vibration of the header at 2 points was tested under the stationary header movement and harvested in the field conditions. The X direction of the test was set to represent the amplitude of the upper and lower vibration of the front header; the Y direction represented the amplitude of the vibration in the left and right direction; the Z direction represented the amplitude of the front and rear vibration.

2.6. Field Rice Stem Cutting Test. In order to study the influence of the header's vibration on cutting the rice stems, the above design parameters were selected and used to test the intrinsic essential relationship between the short stalk and the vibration of the header. The forward speed of the rice combine harvester was set to 0.6~1.0 m/s, and the header used a half-width rice stem cutting method to test the cutting effect of the cutting stalk.

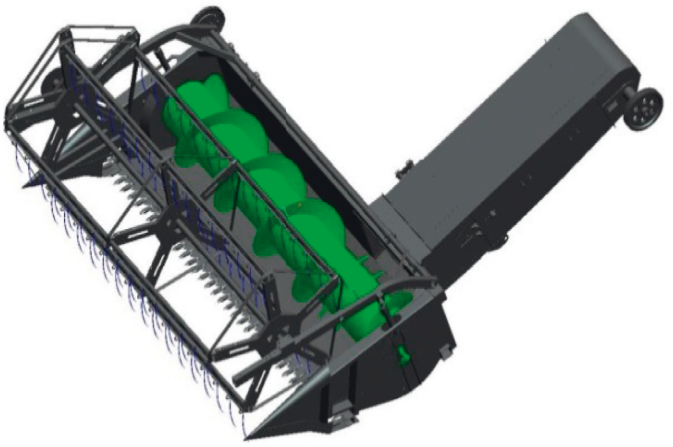

(a)

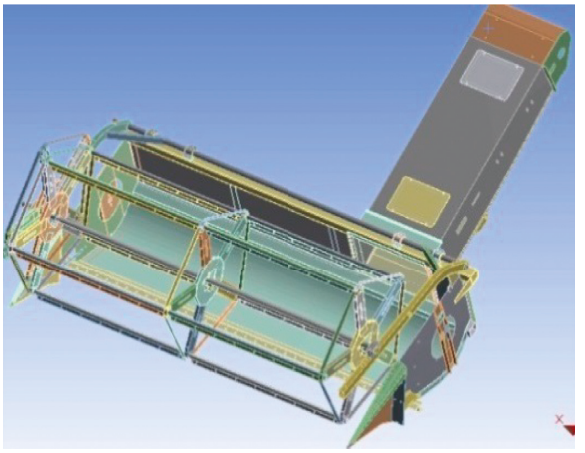

(b)

Figure 10: Assembly device model of the front header. (a) 3D model in Pro/E. (b) Import mode in ANSYS.

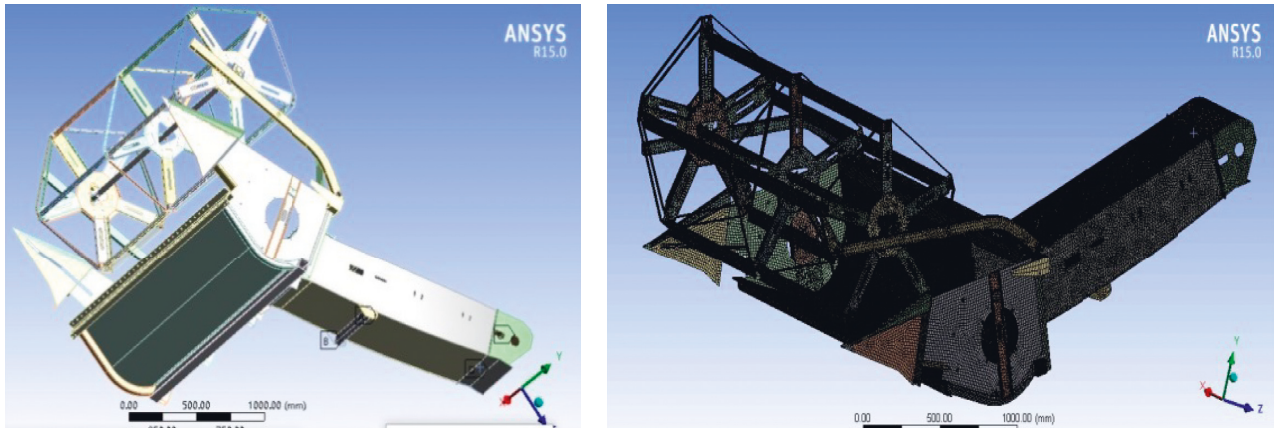

(a) (b)

Figure 11: (a) Constraint positions at frame beam and (b) mesh model of the front header.

Figure 12: Front header physical map.

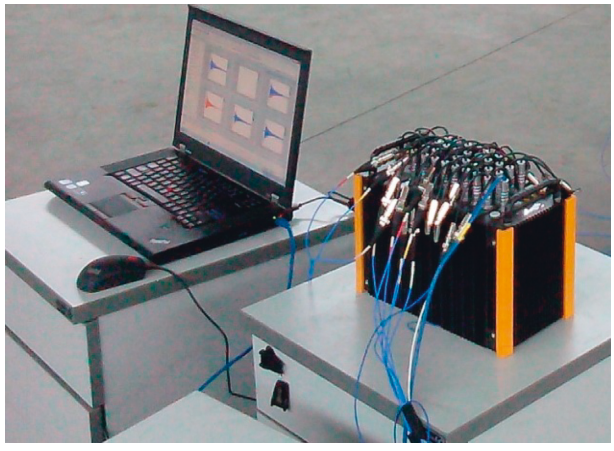

Figure 13: Dynamic signal acquisition instrument.

3. Results and Discussion

3.1. Inherent Modals of Front Header. In order to obtain a more reasonable structural mode of front header, the transmission device of front header was deleted. The structure of front header was simplified. The inherent modals of front header were simulated by ANSYS software. The modal shapes under restricted modality are shown in Figure 16. The mode shapes mainly appeared on pentagonal reel and divider.

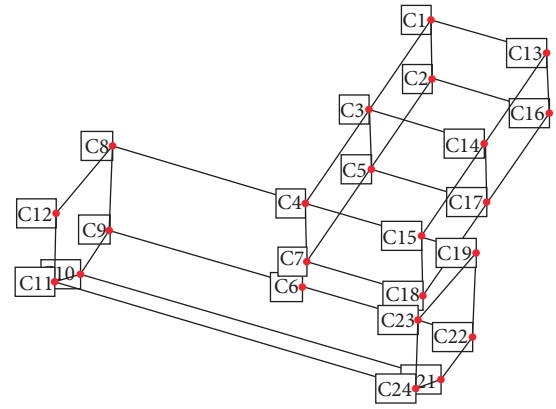

(a)

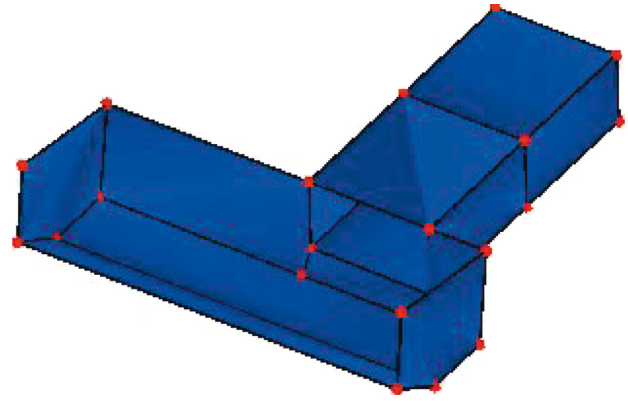

(b)

Figure 14: Frame model of header platform and conveyer house. (a) Line model. (b) Contour model.

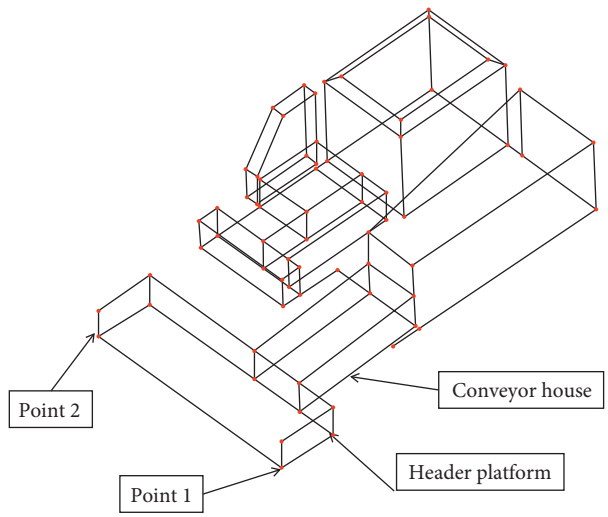

Figure 15: Two vibration test points on the front header.

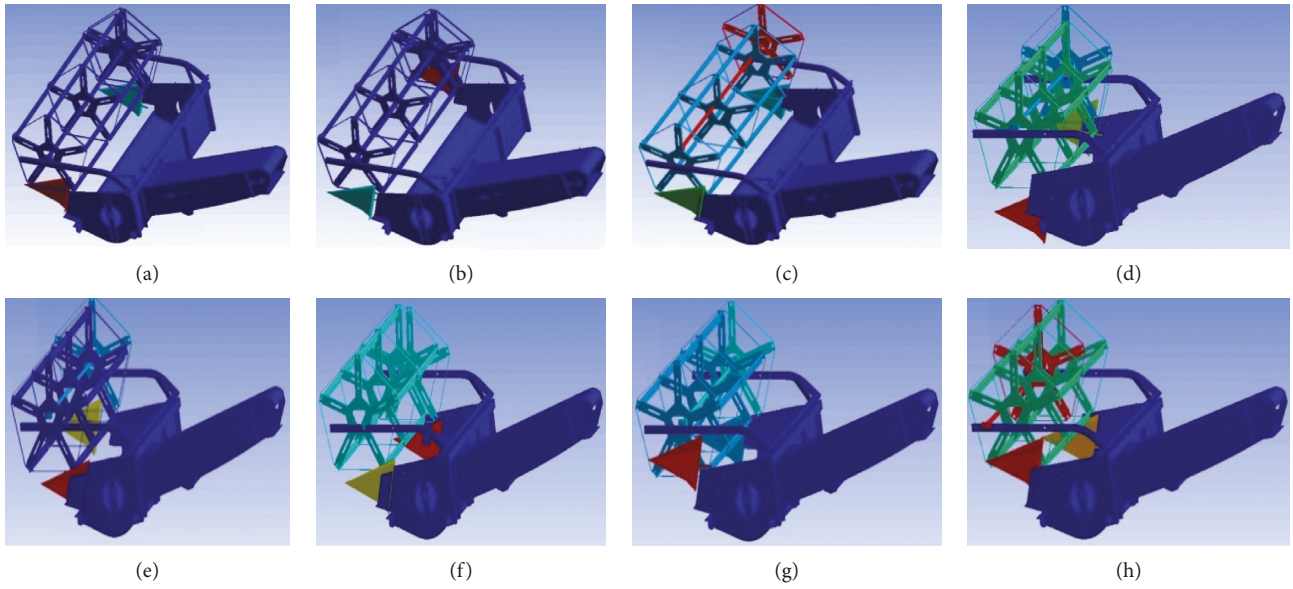

Figure 16: Modal shapes under restricted modality. (a) 1st modal shape. (b) 2nd modal shape. (c) 3rd modal shape. (d) 4th modal shape. (e) 5th modal shape. (f) 6th modal shape. (g) 7th modal shape. (h) 8th modal shape.

According to Figure 16, the 1st intrinsic constraint frequency of front header was 5.28 Hz, and its corresponding mode shape was left and right vibration of the divider. The maximum amplitude of the mode shape on divider side was about 10.09 mm. The frequencies from the 2nd inherent frequency to the 8th inherent constraint frequency were 5.64, 20.28, 29.77, 32.36, 33.85, 44.21, and 46.42 Hz, respectively. The modal shapes and amplitude positions are shown in Figure 16. Based on the natural frequency distribution, the vibration mode, mode vibration frequency, and shapes of the front header are shown in Table 1.

According to Figure 16 and Table 1, the frequency of front side plates (divider) at both ends of the header is 5.28–5.64 Hz, and the first natural frequency of the board will cause vibration during the work of the header. In order to avoid the vibration of the two sides of the header, the side plate is replaced with a round steel divider.

3.2. Experiment Mode of Front Header. The signals of acceleration sensors and the hammer were input into the model of software to solve the frequency response curve of the header platform. The conveyer aisle and the steady state diagram of the mode were analyzed by the DH5902 dynamic signal acquisition instrument. Modal mode and modal frequency of header platform and conveyer aisle were obtained by the DH5902 dynamic signal acquisition system. The Modal shapes of the header platform and conveyer aisle are shown in Figure 17.

According to Figure 17, the 1st intrinsic constraint frequency of header platform and conveyer aisle was 23.38 Hz. The corresponding mode shape was up and down vibration of conveyer house. The maximum amplitude of the mode shape on conveyer aisle was 1.76 mm. The frequencies from the 2nd inherent frequency to the 8th inherent constraint frequency were 48.98, 56.45, 78.92, 94.64, 110.75,

Table 1: Mode vibration frequency and shape of front header.

Mode frequency order	Natural frequency (Hz)	Maximum amplitude (mm)	Mode vibration shape
1	5.28	10.09	Left and right vibration of the divider
2	5.64	11.64	Left and right vibration of the divider
3	20.28	15.42	Radial vertical vibration of pentagonal reel
4	29.77	16.54	Radial vertical vibration of pentagonal reel
5	32.36	19.39	Left and right vibration of the divider
6	33.85	27.54	Left and right vibration of the divider
7	44.21	18.84	Left and right vibration of pentagonal reel and divider
8	46.42	24.41	Left and right vibration of pentagonal reel and divider

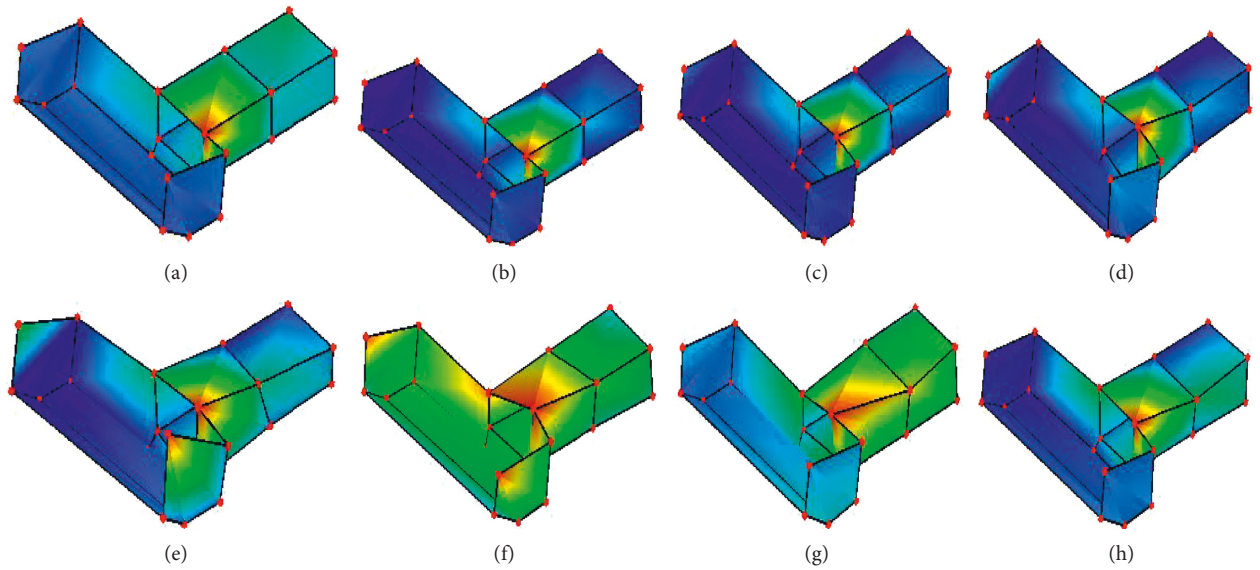

Figure 17: Modal shapes of header platform and conveyer house. (a) 1st modal shape. (b) 2nd modal shape. (c) 3rd modal shape. (d) 4th modal shape. (e) 5th modal shape. (f) 6th modal shape. (g) 7th modal shape. (h) 8th modal shape.

144.12, and 185.02 Hz. The modal shapes and amplitude positions are shown in Figure 17. Based on the natural frequency distribution, the vibration mode, the mode vibration frequency, and shapes of header platform and conveyer aisle are shown in Table 2.

In order to compare the natural frequencies of the various parts of front header and the vibration response characteristics at each frequency, the vibration frequency of header platform, cutting bar, combine auger, pentagon reel, and conveying chain was analyzed. The modal shapes of pentagon reel, combine auger, header platform, and conveyer aisle are shown in Figure 18.

The vibration frequency of header platform, cutting bar, combine auger, pentagon reel, and conveying chain were counted and shown in Table 3.

As shown in Table 3, each intrinsic constraint frequency and modal shapes were different. The vibration frequency of the thin plate position was small, such as combine auger, header platform, conveying aisle, and assembly front header. The frame structure had a high natural frequency. Experiment modal frequency of assembly front header was high natural frequency. Then, the response of the low frequency vibration to the frame excitation was not obvious. As shown in Table 3, the intrinsic frequencies 23.38 Hz, 48.98 Hz, 110.75 Hz, and 144.12 Hz were sensitive response frequencies.

3.3. Frame Vibration of Front Header. There were two points which were selected to characterize the vibration of the header front on the header frame during cutting the rice stem. The vibration signals of point 1 in three directions of *XYZ* are shown in Figure 19.

The maximum and minimum amplitudes, the mean value of the vibration, and the variance of the vibration could be calculated by the vibration signal and the vibration test software. The vibration amplitude test results under various conditions are shown in Table 4.

According to Table 4, the amplitude of point 1 was 18.37~23.49 mm with the mean 0.02~0.04 mm. The average value was less than 0.04 mm, which can be considered that the balance of the vibration was zero. That is to say, the vibration at the static no-load state of the test was steady state. Due to the unstable vibration, the vibration fluctuated greatly, and the variance of the solved vibration mean was 3.07~4.37 mm. The vibration amplitudes of the first point and the second point on the header were not the same. The difference of vibration amplitudes was due to the too long header, which will generate left and right shaking. As shown in Table 4, the vibration of the second point in the front-rear direction was large. The field vibration values of the above headers were similar to those of Reference [30]. As shown in Reference [30], the header vibration was tested during

Table 2: Mode vibration frequency and shape of front header.

Mode frequency order	Natural frequency (Hz)	Maximum amplitude (mm)	Mode vibration shape
1	23.38	1.76	Up and down vibration of conveyer house
2	48.98	1.02	Up and down vibration of conveyer house
3	56.45	0.78	Left and right vibration of conveyer house
4	78.92	0.81	Left and right vibration of conveyer house
5	94.64	0.42	Left and right vibration of left frame side panel
6	110.75	1.68	Whole body vibration of header and conveyer frame
7	144.12	1.17	Left and right vibration of conveyer house
8	185.02	0.31	Left and right vibration of conveyer house

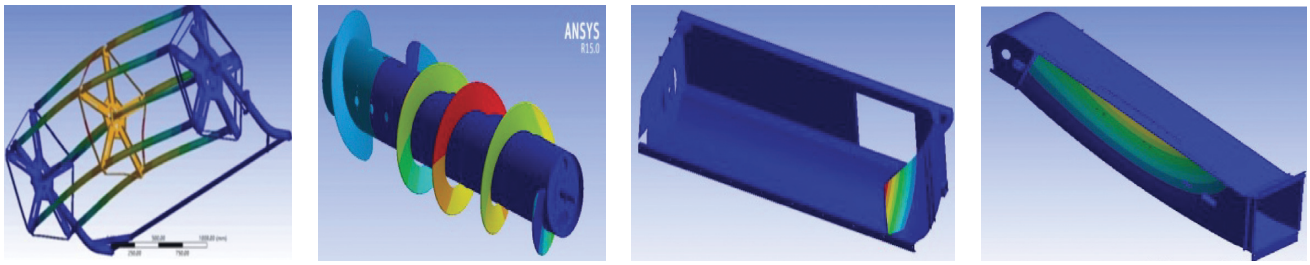

(a) (b) (c) (d)

Figure 18: Modal shapes under restricted modality. (a) Pentagon reel. (b) Combine auger. (c) Header platform. (d) Conveyer aisle.

Table 3: Mode vibration frequency of various parts of front header.

Mode frequency order	Pentagon reel simulation frequency (Hz)	Combine auger simulation frequency (Hz)	Header platform simulation frequency (Hz)	Conveying aisle simulation frequency (Hz)	Simulation frequency of assembly front header (Hz)	Test modal frequency of assembly front header (Hz)
1	20.65	4.96	5.09	8.78	5.28	23.38
2	29.31	5.15	5.13	9.54	5.64	48.98
3	29.81	6.89	12.59	11.42	20.28	56.45
4	35.86	8.34	13.41	13.74	29.77	78.92
5	38.13	14.36	32.27	15.50	32.36	94.64
6	38.18	26.28	33.38	21.12	33.85	110.75
7	39.99	32.18	45.67	21.55	44.21	144.12
8	49.18	63.28	48.55	29.56	46.42	185.02

harvesting in the wheat field. These vibration values were similar features.

When the header worked in the field, the vibration amplitude of the first measuring point on the header in the vertical direction was 25.36 mm, which was significantly higher than no load. However, the vibration of the header in the horizontal and fore-and-rear directions was significantly reduced. When the header worked in the field, the mean value of the vibration increased to 0.12~0.32 mm significantly, but the variance of the mean became smaller. It can be concluded that the vibration of the cutting stalk in the header field was random, and the mean value of the vibration had a tendency to deviate from the origin. However, due to the influence of the stem characteristics, the vibration fluctuation and variance of the mean of the header became smaller. The vibration response of point 2 on the header increased, mainly because the point was far from the trough. When the header was cutting in rice, the vibration amplitude, mean value, and variance of the first and second measurement points were similar.

According to the vibration signals, the vibration analysis software performed FFT (fast Fourier transformation) on the vibration signal to obtain the spectrum of the vibration values. The four orders of vibration frequency are shown in Table 5.

As shown in Table 5, the first-order vibration frequency of the two measuring points was high-frequency. When the header was unloaded, the first-order vibration frequency was 91.79 Hz. The natural frequency of the structure was different. The second-order natural frequency, 31.25 Hz, was closer to the combine auger simulation frequency 32.18 Hz. The third-order natural frequency 15.63 Hz was closer to the conveying aisle simulation frequency 15.50 Hz. Other frequencies are high frequencies, such as 515.63 Hz, 347.63 Hz, and 232.42 Hz. Such high frequency vibrations should be related to the random excitation of the drive sprocket or ground on the header structure. The vibration frequency of the header was significantly higher than the vibration frequency of the header, which was stationary and no load. These vibration frequencies were affected by the random excitation of the ground and the excitation characteristics of the stem cutting.

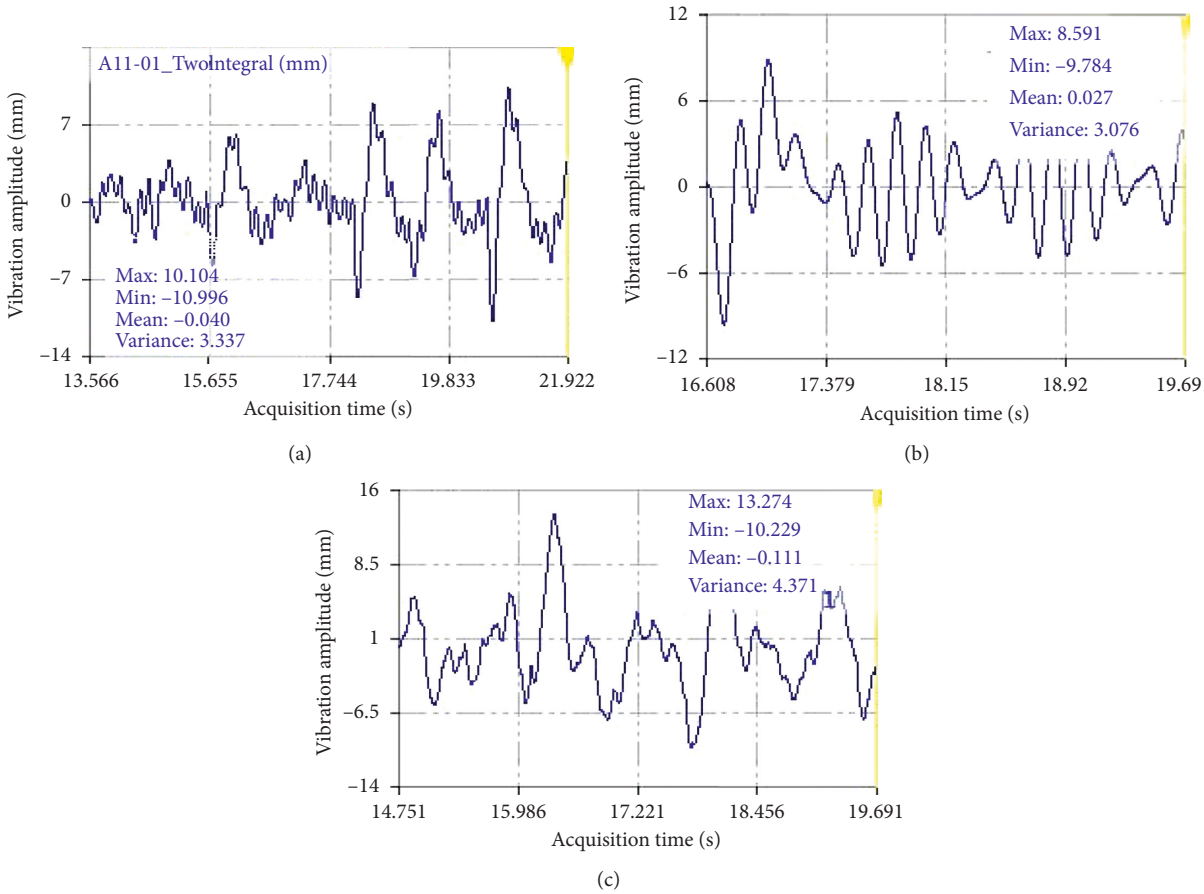

Figure 19: Vibration signal of *X*-*Y*-*Z* direction. (a) *X* direction signal. (b) *Y* direction signal. (c) *Z* direction signal.

Table 4: Vibration amplitude test results at 2 points.

Test point	Static idling vibration value (mm)				Walking harvesting (mm)			
	Maximum	Minimum	Mean	Variance	Maximum	Minimum	Mean	Variance
1*X*	10.10	−10.99	−0.04	3.33	13.62	−11.74	0.14	1.64
1*Y*	8.59	−9.78	−0.02	3.07	6.25	−6.43	0.22	1.48
1*Z*	13.27	−10.22	0.02	4.37	6.64	−11.40	0.12	1.66
2*X*	9.34	−12.47	−0.02	3.27	13.34	−10.67	0.18	1.82
2*Y*	9.90	−17.15	−0.04	3.86	12.48	14.37	0.26	1.64
2*Z*	18.41	−16.01	0.02	3.48	18.02	16.71	0.32	1.79

Table 5: Frequency response test results at 2 points.

Test point	Static idling vibration value (Hz)				Walking harvesting (Hz)			
	1st	2nd	3rd	4th	1st	2nd	3rd	4th
1*X*	91.79	31.25	15.63	517.57	515.63	347.66	669.92	365.23
1*Y*	31.25	15.63	91.79	46.87	515.63	541.02	31.25	15.63
1*Z*	509.76	365.23	91.79	515.63	365.23	513.67	537.11	496.09
2*X*	91.79	15.63	44.93	1.96	232.42	546.88	582.03	537.11
2*Y*	91.79	46.86	15.63	31.25	582.03	64.46	546.88	541.02
2*Z*	91.79	15.63	11.72	751.84	574.22	171.22	582.03	226.56

3.4. Rice Stem Cutting in Field. The cutting stage of the front header was tested at speeds of 0.6, 0.8 and 1.0 m/s. The cutting effects of the stem under different cutting speeds of the header are shown in Figure 20.

When the rice stalks were cut by the header, the height of the stalk and the angle of the cut surface were tested. The short stalks produced by cutting repeatedly were collected. And the length interval and distribution of the short stalks were counted.

(a) (b) (c)

Figure 20: Stem cutting effect at different forward speeds: (a) 0.6 m/s, (b) 0.8 m/s, and (c) 1.0 m/s.

As shown in Figure 20(a), when the heading speed is 0.6 m/s, the cut rice stalks are uneven. There are more short stalks on the ground [31]. As shown in Figure 8, the stem cutting will be located in the II region of the cutting map. So, the stem will be repeatedly cut with a forward speed of 0.6 m/s. The reason of stalks cutting repeatedly is the moving knife, which moves twice in the forward direction of the header. In short, when the forward speed is less than the cutting frequency of the cutter reciprocating, the stem will be repeatedly cut. So, a large number of stems will be repeatedly cut and form into broken stalks. The rice stems formed by repeated cutting are shown in Figure 21.

As shown in Figure 20(b), when the cutting speed is 0.8 m/s, the height of the rice stems cut by the cutter is relatively flat. The number of broken stems is small. Therefore, the forward speed of 0.8 m/s is an ideal advance speed of the cutter.

As shown in Figure 20(c), when the cutting speed of the cutter is 1.0 m/s, the rice stalk are cut neatly. There are fewer broken stalks on the ground. The cut end faces of rice stalks have different degrees of slopes. The results of cutting surface angle are shown in Figure 22.

As shown in Figure 21, the length of the repeatedly cut stems was normally distributed. The length of the cut stems was distributed between 14.20 and 45.40 mm, which the mean length was 23.60 mm. This length is inextricably linked to the up and down vibration of the header. As shown in Table 4, when the header was in the cutting work, the header was vibrated up and down by 25.36 mm. The peak-to-peak value of the upper and lower vibration of the header was similar to the length of the stem being repeatedly cut with an error of 7.46%. If the header does not vibrate up and down during cutting, the cutter will not produce short stalks. In the actual cutting process, the cutter was vibrating up and down, so the cutter produces short stalks. From the theoretical cutting, the length of the short stalk was the peak-to-peak (upper and lower) vibration value.

As shown in Figure 22, when the cutting head advance speed was 1.0 m/s, the cutting head forward speed was faster than the cut frequencies. More stems were less likely to be cut or pushed to be cut. According to the stem oblique cutting principle shown in Figure 9, there were three types of bevel angles, 38°, 44°, and 62°, which were cut by the header. The cutting surface angle (62°) was mainly caused by the faster forward speed. The faster forward speed causes the slope to be cut when the stem was cut. The cutting surface 44° was caused by the repeated cutting zone II in the main cutting diagram. Stalk was also inclined when it was cut for the second time. The cutting surface 38° was caused by the missing cutting zone III in the main cutting diagram. So, the faster forward speed causes the stem to be cut obliquely.

4. Conclusion

(1) The vibration amplitude of one side of header was 18.37~23.49 mm with the mean 0.02~0.04 mm. The mean vibration value is less than 0.04 mm, which can be considered that the balance of the vibration is zero at no-load state. The frame structure has a high natural frequency than the thin plate position.

(2) When the header was cutting rice, the vibration amplitude, mean value, and variance of the first and second measurement points were the similar. The length of the cut stems was distributed between 14.20 and 45.40 mm; the mean length is 23.60 mm. This length is inextricably linked to the up and down vibration of the header 25.36 mm. The peak-to-peak value of the upper and lower vibration was similar to the length of the stems which were cut repeatedly.

(3) The cutting surface angle (62°) was mainly caused by the faster forward speed. The cutting surface 44° was caused by the repeated cutting zone II in the main cutting diagram. The cutting surface 38° was caused by the missing cutting zone III in the main cutting diagram. The faster forward speed causes the stem

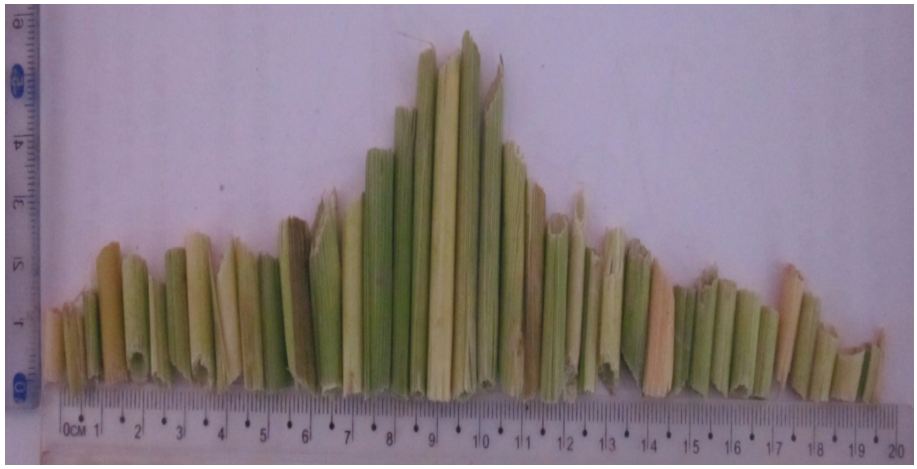

Figure 21: Interval length distribution and distribution of short stems of rice.

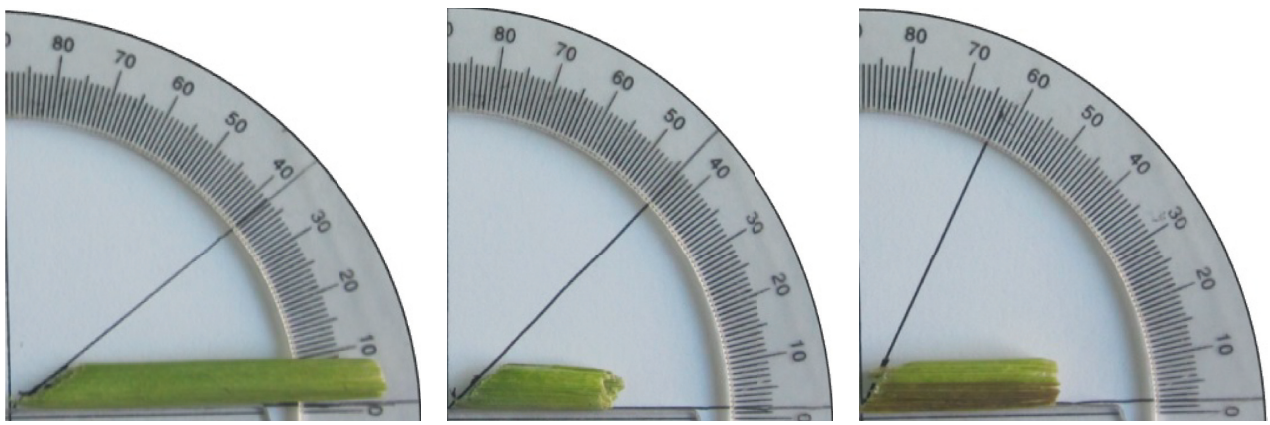

(a) (b) (c)

Figure 22: Cutting surface angle of stems at different forward speeds. (a) Surface angle 38°. (b) Surface angle 44°. (c) Surface angle 62°.

to be cut obliquely. If height of the rice stems cut by the cutter should be relatively flat, the forward speed of 0.8 m/s is an ideal advance speed of the cutter.

Data Availability

The data used to support the findings of this study are available from the corresponding author upon request.

Conflicts of Interest

The authors declare that they have no conflicts of interest.

Acknowledgments

This research work was supported by the National Natural Science Foundation of China (51705212), the Natural Science Foundation of Jiangsu Province (BK20170553), the National Key Research and Development Plan (2016YFD0702004), and a project funded by the Priority Academic Program Development of Jiangsu Higher Education Institutions (PAPD).

References

[1] Y. L. Wang, Y. Zeng, L. K. Xu, J. X. Sun, and M. Zhao, "Establishing the shafting vibration model under the condition of spindle torsional deformation," *Journal of Drainage and Irrigation Machinery*, vol. 37, no. 7, pp. 600–605, 2018.

[2] S. Jiang, W. Yao, J. Chen, and T. Cai, "Finite element modeling of FRP-strengthened RC beam under sustained load," *Advances in Materials Science and Engineering*, vol. 2018, Article ID 7259424, 16 pages, 2018.

[3] Z. Tang, Y. M. Li, R. Wang, and J. S. Chen, "Experimental study of multi-source dynamic load of combine harvester in rice harvesting," *International Agricultural Engineering Journal*, vol. 25, no. 3, pp. 46–52, 2016.

[4] B. Bai and L. X. Zhang, "Dynamic response of hydro-turbine set shaft system under stochastic hydraulic excitation," *Journal of Drainage and Irrigation Machinery*, vol. 35, no. 5, pp. 398–403, 2017.

[5] Q. Guo, X. L. Zhang, Y. F. Xu, P. P. Li, C. Chen, and H. W. Xie, "Simulation and experimental study on cutting performance of tomato cane straw based on EDEM," *Journal of Drainage and Irrigation Machinery*, vol. 30, no. 10, pp. 1017–1022, 2018.

[6] R. Ebrahimi, M. Esfahanian, and S. Ziaei-Rad, "Vibration modeling and modification of cutting platform in a harvest combine by means of operational modal analysis (OMA)," *Measurement*, vol. 46, no. 10, pp. 3959–3967, 2013.

[7] S. Chuan-Udom, "Development of a cutter bar driver for reduction of vibration for a rice combine harvester," *Asia-Pacific Journal of Science and Technology*, vol. 15, no. 7, pp. 572–580, 2017.

[8] T. Fukushima, E. Inoue, M. Mitsuoka, T. Okayasu, and K. Sato, "Collision vibration characteristics with interspace in knife driving system of combine harvester," *Engineering in Agriculture, Environment and Food*, vol. 5, no. 3, pp. 115–120, 2012.

[9] T. Fukushima, E. Inoue, M. Mitsuoka, M. Matsui, and T. Okayasu, "Vibration characteristics and modeling of knife driving system of combine harvester (Part 2)," *Journal of the Japanese Society of Agricultural Machinery*, vol. 68, no. 5, pp. 59–64, 2006.

[10] Y. X. Yu, Q. D. Meng, Y. L. Li, and W. Mao, "Load spectrum test and fatigue analysis of cutting table frame of 4LZ–4.6 whole–feeding harvester," *Journal of Zhejiang Sci-Tech University (Natural Sciences)*, vol. 35, no. 5, pp. 720–725, 2016.

[11] D. D. Kong, J. Yin, L. Xiao, and K. Zhang, "Simulation analysis and optimal design of the lifting header of combined harvester based on motion," *Machinery Design and Manufacture*, vol. 2, pp. 231–234, 2018.

[12] Y. Liao, Y. Xiang, M. L. Wu, D. W. Liu, Y. Q. Cheng, and Y. L. Li, "Design and test of the adaptive height adjustment system for header of the combine–harvester," *Journal of Hunan Agricultural University (Natural Sciences)*, vol. 44, no. 3, pp. 326–329, 2018.

[13] Y. N. Li, Y. W. Yi, S. W. Du, Q. S. Ding, and W. M. Ding, "Design and experiment on air blowing header of plot combine harvester for grain," *Transactions of the CSAE*, vol. 48, no. 6, pp. 79–87, 2017.

[14] Y. Li, X. L. Zhang, Q. Dan, and B. Xu, "The finite element modal analysis of the frame of cutting table on 4LZ–2.0 rice and wheat combine harvester," *Journal of Agricultural Mechanization Research*, vol. 11, pp. 90–93, 2011.

[15] Z. P. Gao, L. Z. Xu, Y. M. Li, Y. D. Wang, and P. P. Sun, "Vibration measure and analysis of crawler-type rice and wheat combine harvester in field harvesting condition," *Transactions of the Chinese Society of Agricultural Engineering*, vol. 33, no. 20, pp. 48–55, 2017.

[16] M. T. Li, J. J. Liu, L. J. Zhu, J. Z. Zhao, and Z. Zha, "Vibration finite element modal analysis of combine harvester header and inclined conveyer," *Journal of Chinese Agricultural Mechanization*, vol. 38, no. 7, pp. 10–16, 2017.

[17] X. J. He, "Upgrade of rice harvester hydraulic system," *Journal of Agricultural Mechanization Research*, vol. 11, pp. 74–79, 2018.

[18] K. Lu, G. Z. Zhang, S. B. Peng et al., "Design and performance of tracked harvester for ratoon rice with double-headers and double threshing cylinders," *Journal of Huazhong Agricultural University*, vol. 36, no. 5, pp. 108–114, 2017.

[19] S. Chuan-Udom, T. Srison, and W. Wiangwisad, "Comparative study on vibration of a combine harvester due to operation of cutter bar driver, reel, and auger," *TSAE Journal*, vol. 15, no. 1, pp. 3–6, 2009.

[20] M. Liang, "Optimization design for structure reliability of cutting table wheat harvester based on improved particle swarm optimization algorithm," *Journal of Agricultural Mechanization Research*, vol. 2, pp. 52–56, 2017.

[21] S. G. Ren, F. Jiao, M. L. Wu, S. Z. He, and S. Z. Tang, "Studies of united harvest machine cutting system structure parameters on the vibration impact," *Journal of Agricultural Mechanization Research*, vol. 11, pp. 38–43, 2018.

[22] Z. Tang, Y. M. Li, and C. H. Wang, "Experiments on variable-mass threshing of rice in the tangential-longitudinal-flow combine harvester," *Journal of Agricultural Science and Technology*, vol. 15, no. 4, pp. 1319–1334, 2013.

[23] Z. Tang, Y. Li, L. Xu, and F. Kumi, "Modeling and design of a combined transverse and axial flow threshing unit for rice harvesters," *Spanish Journal of Agricultural Research*, vol. 12, no. 4, pp. 973–983, 2014.

[24] C. Y. Chen, X. Z. Wang, and Z. F. He, "Design of header for rape harvesting using grain combine harvester," *Transactions of the Chinese Society of Agricultural Engineering*, vol. 34, no. 5, pp. 54–60, 2003.

[25] Z. Tang, H. T. Zhang, and Y. P. Zhou, "Unbalanced vibration identification of tangential threshing cylinder induced by rice threshing process," *Shock and Vibration*, vol. 2018, Article ID 4708730, 14 pages, 2018.

[26] Y. Shi, X. Zhang, S. Cui, and K. Ma, "Contact forces in a screw feeding process," *Advances in Materials Science and Engineering*, vol. 2018, Article ID 4924582, 6 pages, 2018.

[27] X. X. Xiao, H. Li, X. D. Qi, and M. Wang, "Modal and transient analysis of threshing cylinder based on ANSYS Workbench," *Journal of Agricultural Mechanization Research*, vol. 8, pp. 46–50, 2016.

[28] L. J. Yao, W. D. Cao, X. Jiang, Q. Zhang, and Y. M. Xu, "FEA for rotor system of axial flow pump based on ANSYS," *Journal of Drainage and Irrigation Machinery*, vol. 37, no. 7, pp. 612–617, 2018.

[29] L. Bai, Y. Li, M. Yang, Z. Yao, and Z. Yao, "Influences of process parameters and vibration parameters on the forming force in the ultrasonic-assisted incremental forming process," *Advances in Materials Science and Engineering*, vol. 2018, Article ID 5726845, 12 pages, 2018.

[30] Z. Tang, Y. M. Li, and J. B. Liu, "Dynamic vibration test and analysis of 4LZ-2.5B combine harvester cutting table rack in wheat harvesting," *International Agricultural Engineering Journal*, vol. 26, no. 1, pp. 79–86, 2017.

[31] Z. Tang, Y. Li, Z. Zhao, and T. Sun, "Structural and parameter design of transverse multi-cylinders device on rice agronomic characteristics," *Spanish Journal of Agricultural Research*, vol. 13, no. 4, article e0216, 2015.